Anterior insular cortex inputs to the dorsolateral striatum govern the maintenance of binge alcohol drinking

David L. Haggerty[1], Braulio Muñoz[1], Taylor Pennington[1], Gregory G. Grecco[1,2], Brady K. Atwood[1,3*]

Affiliations:

[1]Department of Pharmacology & Toxicology, Indiana University School of Medicine; Indianapolis, IN 46202, USA.
[2]Medical Scientist Training Program, Indiana University School of Medicine, Indianapolis, IN 46202
[3]Stark Neurosciences Research Institute, Indiana University School of Medicine; Indianapolis, IN 46202, USA.

*Corresponding author. Email: bkatwood@iu.edu

Abstract

How does binge drinking alcohol change synaptic function, and do these changes maintain binge consumption? The anterior insular cortex (AIC) and dorsolateral striatum (DLS) are brain regions implicated in alcohol use disorder. In mice, we found that binge drinking alcohol produced glutamatergic synaptic adaptations selective to AIC inputs within the DLS. Photoexciting AIC→DLS circuitry during binge drinking decreased alcohol, but not water consumption and altered alcohol drinking mechanics. Further, drinking mechanics alone from drinking session data predicted alcohol-related circuit changes. AIC→DLS manipulation did not alter operant, valence, or anxiety-related behaviors. These findings suggest that alcohol-mediated changes in AIC inputs govern behavioral sequences that maintain binge drinking and may serve as a circuit-based biomarker for the development of alcohol use disorder.

Introduction:

Binge alcohol consumption, defined as consuming four to five or more drinks per drinking session, represents a large proportion of the deaths associated with problematic alcohol use and alcohol use disorder (AUD) (Mokdad et al. 2004; Kanny et al. 2018). Binge drinking is particularly prevalent amongst young adults, is behaviorally conserved in rodents, and is a theoretical entry point to the addiction cycle (Thiele and Navarro 2014; Patrick et al. 2013; Chung et al. 2018; Koob and Volkow 2010). Ultimately, partaking in binge drinking is one of the strongest predictors for developing AUD (Addolorato et al. 2018).

How alcohol alters neural circuitry that underlies binge drinking remains poorly understood. Previous work has shown binge drinking alters glutamate receptor function across many brain regions (Hwa, Besheer, and Kash 2017). Only a few neural circuits, such as the ventral tegmental area and thalamic inputs to the extended amygdala, locus coeruleus outputs to lateral hypothalamus and rostromedial tegmental nucleus, and medial prefrontal cortex inputs to the periaqueductal gray have been directly linked to the behavioral control of binge alcohol drinking (Rinker et al. 2017; Ferguson et al. 2019; Levine et al. 2021; Dornellas et al. 2021; Burnham et al. 2021; Siciliano et al. 2019). The insular cortex is an interoceptive brain region that regulates many components of drug use and is implicated in AUD (Centanni et al. 2021; Gogolla 2017). The dorsal striatum, and in particular the dorsolateral striatum (DLS) is a principal brain region involved in the development of habit learning, drug consumption and seeking behaviors, and is also involved in the development of AUD (Barker et al. 2015). We sought to better understand the impact that binge alcohol consumption has on glutamatergic synaptic plasticity at anterior insular cortex (AIC) inputs to the DLS and how these synapses regulate binge alcohol consumption. We previously showed that synaptic plasticity at these AIC→DLS synapses is uniquely vulnerable to disruption by alcohol exposure, relative to other glutamate synapses within the same brain subregion (Munoz et al. 2018). In addition, while these synapses have been investigated anatomically and functionally, they have yet to be behaviorally evaluated in any context (Hunnicutt et al. 2016; Munoz et al. 2018; Munoz, Haggerty, and Atwood 2020; Wall et al. 2013).

Results and Discussion:

We isolated AIC→DLS circuitry by injecting an anterograde adeno-associated virus (AAV) into the AIC, utilizing the CaMKIIa promoter to drive expression of channelrhodopsin-2 (ChR2) tagged with enhanced yellow fluorescent protein (EYFP) to visualize and modulate glutamatergic AIC inputs within the DLS (**Figure 1A and supplemental figure 1**). Animals then underwent three weeks of the Drinking in the Dark (DID) paradigm where they had 0, 2, or 4 hours of access to alcohol or water each day, which produced “binge-like” levels of alcohol intake as measured by a positive correlation between alcohol intake and blood alcohol concentration (BAC) with a subset of animals achieving BACs greater than 0.08 mg% (**Figure 1B-D and supplemental figure 2**) (Thiele and Navarro 2014). Twenty-four hours after the last DID session, acute slices of the DLS were made to measure AIC-mediated synaptic responses.

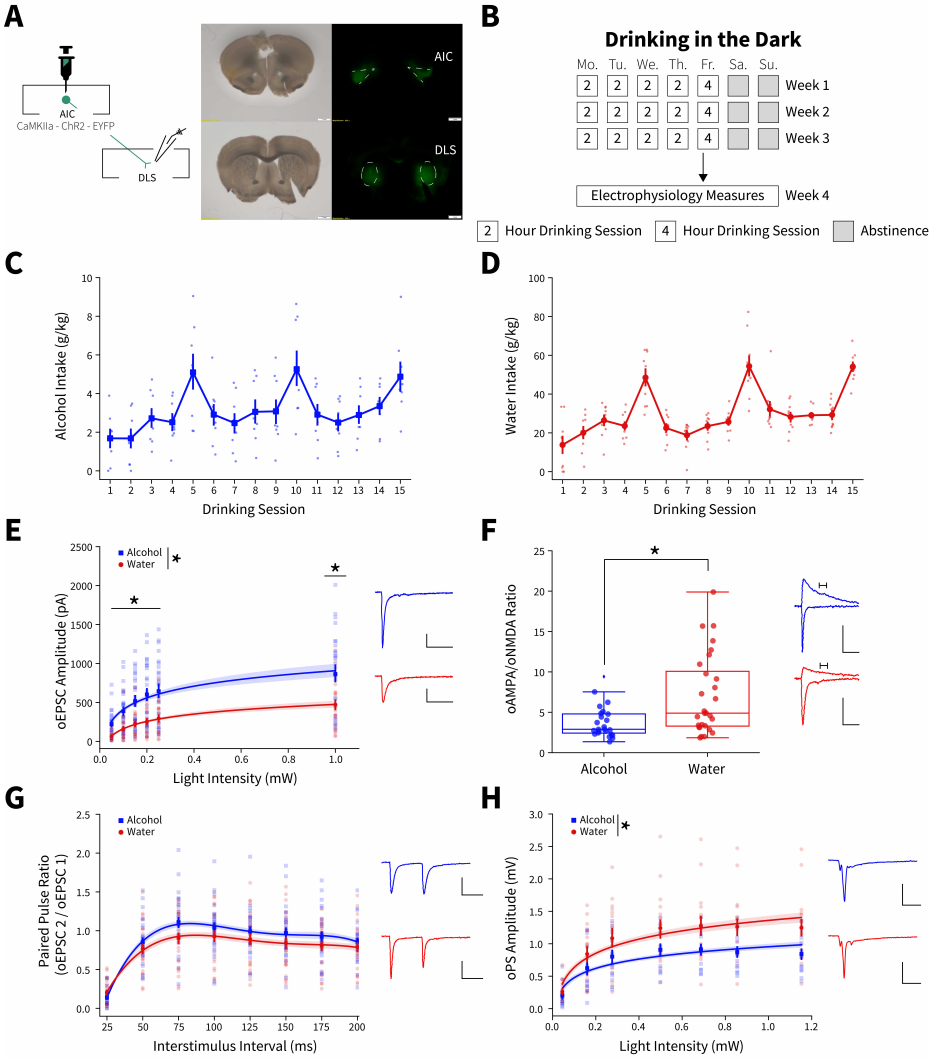

Figure 1 Binge alcohol consumption alters synaptic plasticity of anterior insular cortex inputs (AIC) to the dorsolateral striatum (DLS).
(A) Representation of viral strategy and expression to record AIC input responses within the DLS (**B**) Schematic of Drinking in the Dark (DID) protocol for electrophysiology experiments. (**C**) Group and individual animals' alcohol consumption (n = 8 animals). (**D**) Group and individual animals' water consumption (n = 10 animals). (**E**) Binge alcohol consumption increased optically-evoked post-synaptic current (oEPSC) amplitude of AIC inputs within the DLS (two-way mixed analysis of variance (ANOVA), Fluid $F_{(1,50)} = 15.6084$, $p = 0.0002$; Fluid x Light Intensity $F_{(5,250)} = 6.0674$, $p = 0.000025$; alcohol: 26 recordings, n = 5 animals; water: 26 recordings, n = 6 animals). (**F**) Binge alcohol consumption reduced optically-evoked AMPA (oAMPA) to NMDA (oNMDA) glutamate receptor current ratios (Mann-Whitney, $U = 189$, $p = 0.0072$; alcohol: 24 recordings, n = 5 animals; water: 28 recordings, n = 6 animals). (**G**) There was no main effect of binge alcohol consumption on paired-pulse ratios of oEPSCs (oPPR) compared to water consumption (two-way mixed analysis ANOVA, Fluid $F_{(1,55)} = 2.1158$, $p = 0.1515$). However, there was a significant fluid by interstimulus interval interaction (Fluid x Light Intensity $F_{(7,385)} = 2.6912$, $p = 0.0099$; alcohol: 26 recordings, n = 5 animals; water: 26 recordings, n = 6 animals). (**H**) Binge drinking alcohol decreased optically-evoked population spike amplitudes (oPS) produced by photoexciting AIC inputs within the DLS (two-way mixed ANOVA, Fluid $F_{(1,28)} = 4.3484$, $p = 0.0463$; Fluid x Light Intensity $F_{(6,168)} = 2.9574$, $p = 0.0090$; alcohol: 14 recordings, n = 4 animals; water: 16 recordings, n = 6 animals). Error bars and shading indicate ± SEM. Box plot whiskers represent inter-quartile range.

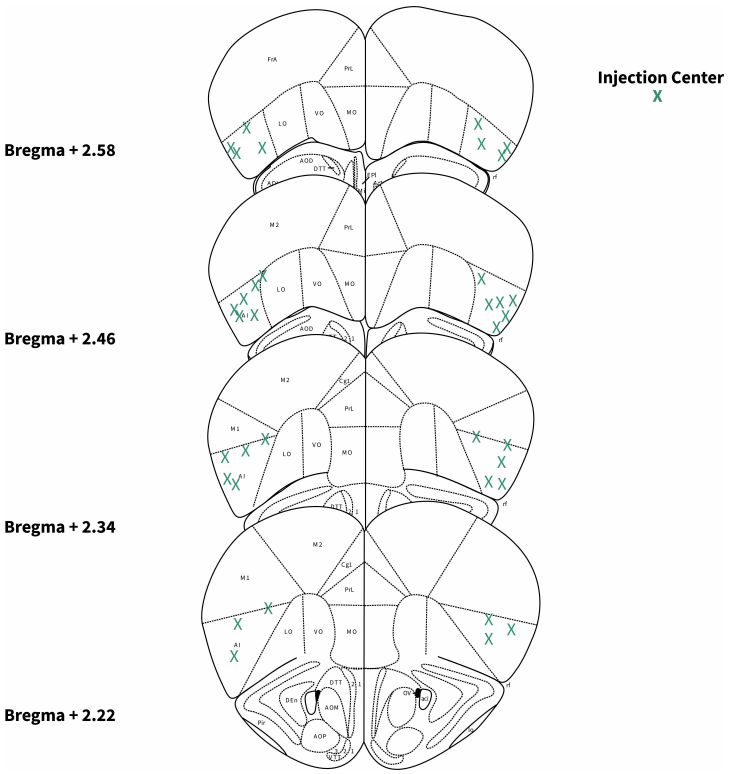

Supplemental Figure 1. Locations of AIC injections for DLS electrophysiology.
Bilateral injection centers of AAV-ChR2-EYFP in the AIC as verified by histology (alcohol: n = 8 animals; water: n = 10 animals).

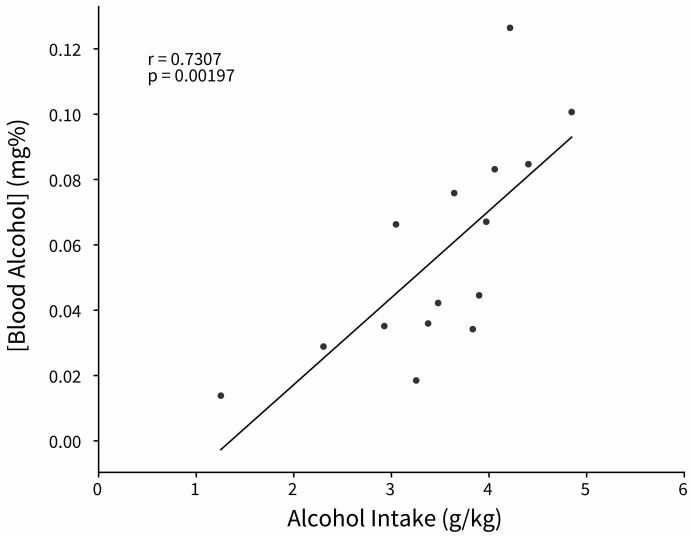

Supplemental Figure 2. Binge alcohol consumption is positively correlated with blood alcohol concentration.
Alcohol intake was measured from a 2 hour DID session and retro-orbital blood samples were collected within 30 minutes of the completion of the session to calculate blood alcohol concentration (Pearson's correlation, r = 0.7307, p = 0.00197).

An input-output assessment of optically-evoked excitatory postsynaptic currents (oEPSCs) recorded from DLS medium spiny neurons (MSNs) at increasing light intensities showed that alcohol drinking animals had greater oEPSC amplitudes than water controls (**Figure 1E**). Binge drinking also decreased optically-evoked AMPA to NMDA glutamate receptor current ratios (oAMPA /oNMDA) (**Figure 1F**). Given that the increased oEPSCs measured with our input-output assessment (**Figure 1E**) were likely AMPA receptor-mediated, we interpret the decrease in oAMPA /oNMDA ratio to mean that alcohol consumption has a larger effect on NMDA receptor currents than AMPA receptor currents. Assessing paired-pulse ratios of oEPSCs (oPPR) at increasing interstimulus intervals revealed a significant fluid by interstimulus interval interaction (**Figure 1G**). A change in PPR is usually interpreted as an altered neurotransmitter release probability (Jackman and Regehr 2017). Therefore, these PPR data indicate alcohol consumption may alter glutamate release probability from AIC inputs within the DLS. There were no differences in spontaneous glutamatergic synaptic activity between water and alcohol drinkers in the DLS (**Supplemental figure 3A-D**). Consistent with previous findings, we have shown that alcohol can have synapse-specific effects in dorsal striatum, which are otherwise obscured by the net effects at other synapses when synaptic transmission is measured in a non-specific manner (Munoz et al. 2018; Munoz, Haggerty, and Atwood 2020). These data suggest the measured alcohol-mediated plasticity changes were selective for AIC inputs. Furthermore, these data indicate that binge drinking alcohol specifically potentiates postsynaptic AMPA and NMDA glutamate receptor responses at AIC→DLS synapses, with a potential modest accompanying decrease in glutamate release.

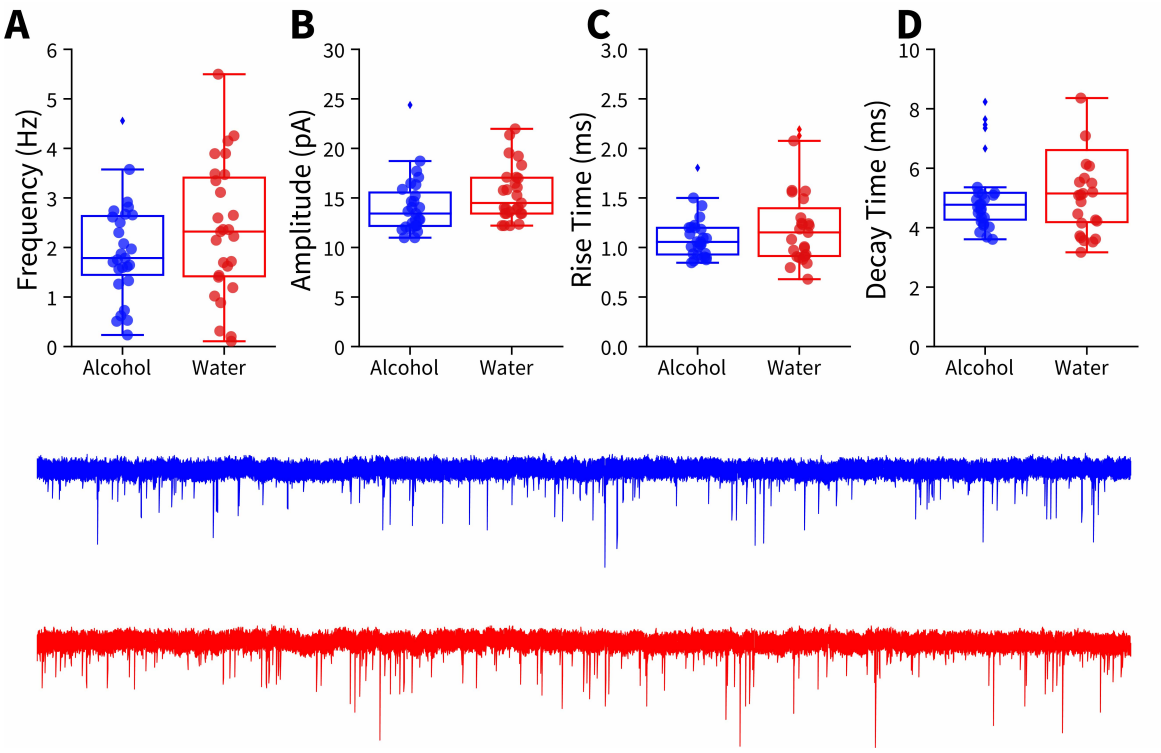

Supplemental Figure 3. Binge alcohol consumption did not alter spontaneous excitatory synaptic activity in the DLS.
Spontaneous excitatory postsynaptic currents (sEPSCs) were measured in DLS medium spiny neurons from mice after 3 weeks of binge alcohol or water consumption. Binge alcohol consumption did not affect sEPSC **(A)** frequency, **(B)** amplitude, **(C)** rise time, or **(D)** decay time (alcohol: 27 recordings, n =6 animals; water: 27 recordings, n = 5 animals).

To investigate the effects of activating AIC inputs on broader DLS network activity, we recorded optically-evoked population spikes (oPS) produced by photoexciting AIC inputs within the DLS at increasing light intensities. oPS amplitudes were decreased in mice that binge drank alcohol compared to water (**Figure 1H**), indicating that the net effect of binge alcohol-induced AIC→DLS synaptic adaptations is a reduced network response to AIC input activation. This is curious as we measured an increased glutamate receptor response (**Figure 1E and 1F**). These data indicate that AIC inputs to DLS may drive local inhibitory networks leading to decreased MSN activity. AIC inputs equally innervate different types of MSNs indicating that this effect is not due to a preferential engagement of one type of MSN (Wall et al. 2013). Other possibilities are that AIC inputs induce feedforward inhibition through local interneurons, such as engaging fast-spiking interneurons, which have been implicated in compulsive alcohol consumption (Patton et al. 2021; Manz et al. 2020). This is a possibility that will need to be explored in future studies.

Alterations in DLS neurotransmission are known to facilitate the development of habit learning in the context of substance-related behaviors and are also associated with the expression of numerous alcohol-related behaviors (Koob and Volkow 2010; Lovinger and Alvarez 2017; Corbit, Nie, and Janak 2012; Patton, Shah, and Mathur 2016). Glutamate receptor signaling specifically within the DLS mediates alcohol seeking behavior (Corbit, Nie, and Janak 2014). We hypothesized that by modulating AIC inputs within the DLS, we could alter ongoing binge drinking behavior. Initially, we predicted that photoexciting AIC inputs during alcohol consumption would increase binge drinking.

We again isolated AIC→DLS circuitry by injecting an AAV-ChR2-EYFP vector or a control vector that solely expressed enhanced green fluorescent protein (eGFP) into the AIC and implanted a wireless optogenetic probe into the DLS to modulate AIC inputs to the DLS during homecage DID sessions (**Figure 2A and supplemental figure 4**) (Shin et al. 2017). Animals then underwent three weeks of water or alcohol DID, via lickometers that monitored liquid intake, to acquire binge alcohol-induced plasticity changes in the absence of optical stimulation (**Figure 2B-C**) (Godynyuk et al. 2019). Licks, bouts, and total lick duration metrics from the lickometers were significantly correlated with water and alcohol intakes and thus provided high-resolution drinking microstructure details about how and when during each DID session each animal consumed water or alcohol (**Supplemental figure 5A-F)**. During binge acquisition (weeks 1 - 3), there were baseline differences between ChR2 and eGFP controls for water, but not alcohol intake (**Figure 2D-E**).

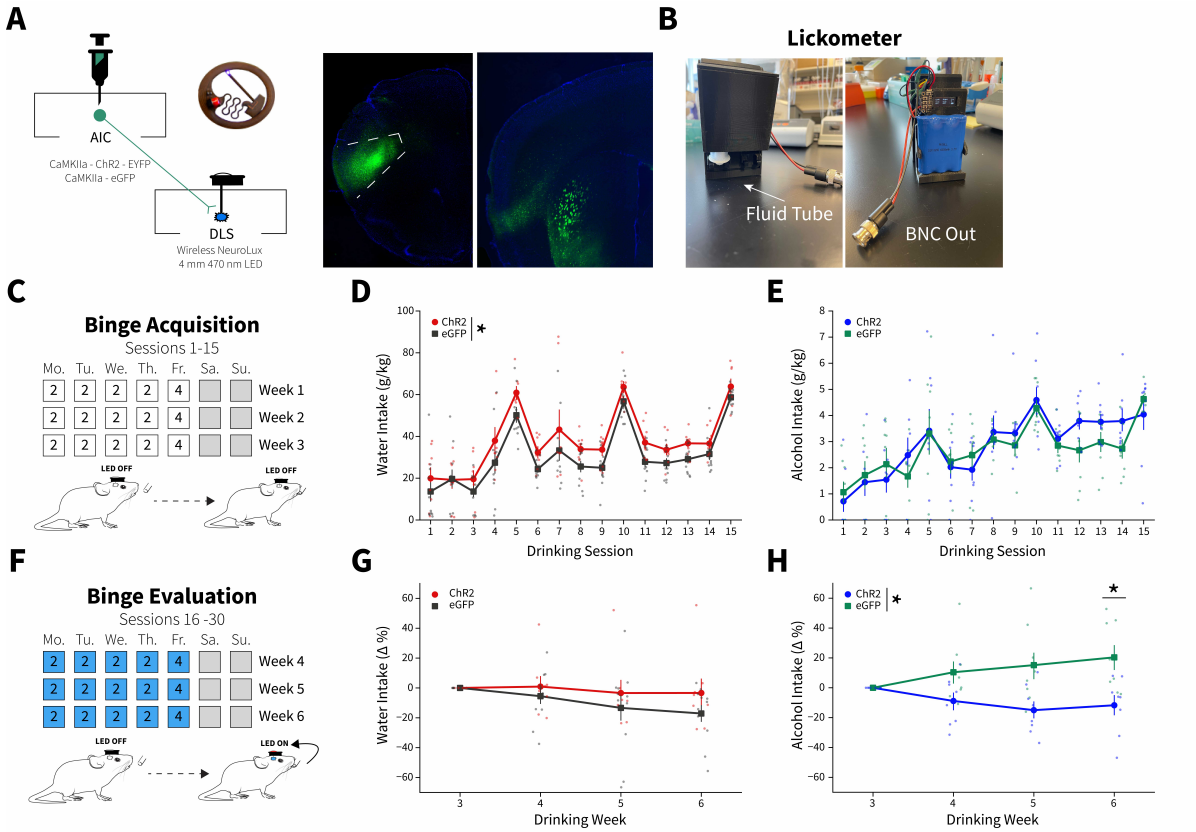

Figure 2 AIC inputs to the DLS modulate binge alcohol intake, but not water intake. (**A**) Representation of viral strategy and expression to modulate AIC inputs within the DLS. (**B**) Photographs and description of lickometer. (**C**) Schematic of DID protocol for binge alcohol or water acquisition. (**D**) Group and individual animals' water consumption differed by viral expression during binge acquisition (two-way mixed ANOVA, Virus $F_{(1,16)} = 8.1951$, $p = 0.0113$; ChR2: n = 8 animals, eGFP: n = 11 animals). (**E**) Group and individual animals' alcohol consumption did not differ by viral expression grouping during binge acquisition (ChR2: n = 8 animals, eGFP: n = 8 animals). (**F**) Schematic of DID protocol for binge alcohol or water evaluation. (**G**) Photoexciting AIC inputs within the DLS during DID not alter water intakes, but (**H**) decreased alcohol intake (two-way mixed ANOVA, Virus $F_{(1,14)} = 8.5743$, $p = 0.0110$; Virus x Drinking Week $F_{(3,42)} = 4.7132$, $p = 0.0063$; Drinking Week 6, p = 0.0281; ChR2: n = 8 animals, eGFP: n = 8 animals). Error bars indicate ± SEM. All post hoc comparisons are Sidak corrected.

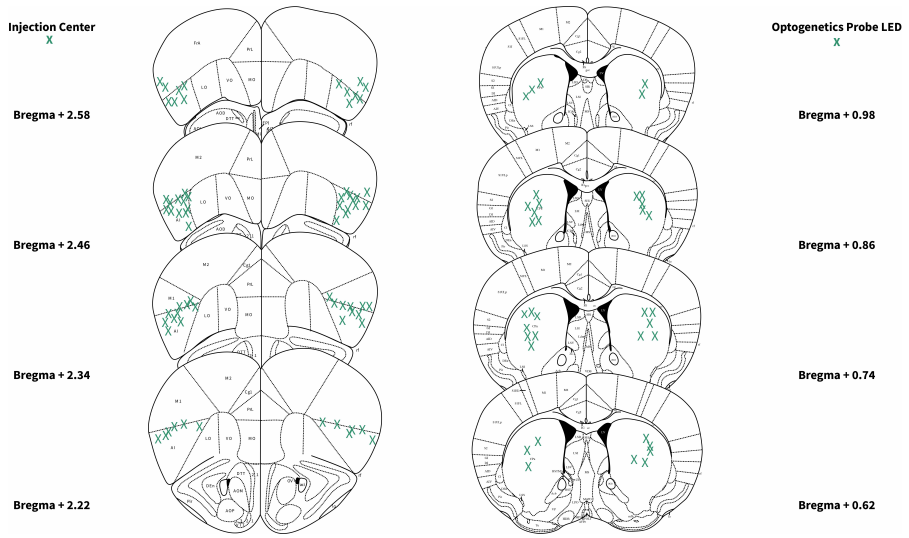

Supplemental Figure 4. Locations of AIC injections and DLS wireless optogenetic probe placements.
Bilateral injection centers of AAV-ChR2-EYFP or AAV-eGFP in the AIC and unilateral (left: n = 18 probes; right: n = 17 probes) wireless optogenetic probe LED locations as verified by histology (alcohol: n = 16 animals; water n = 19 animals).

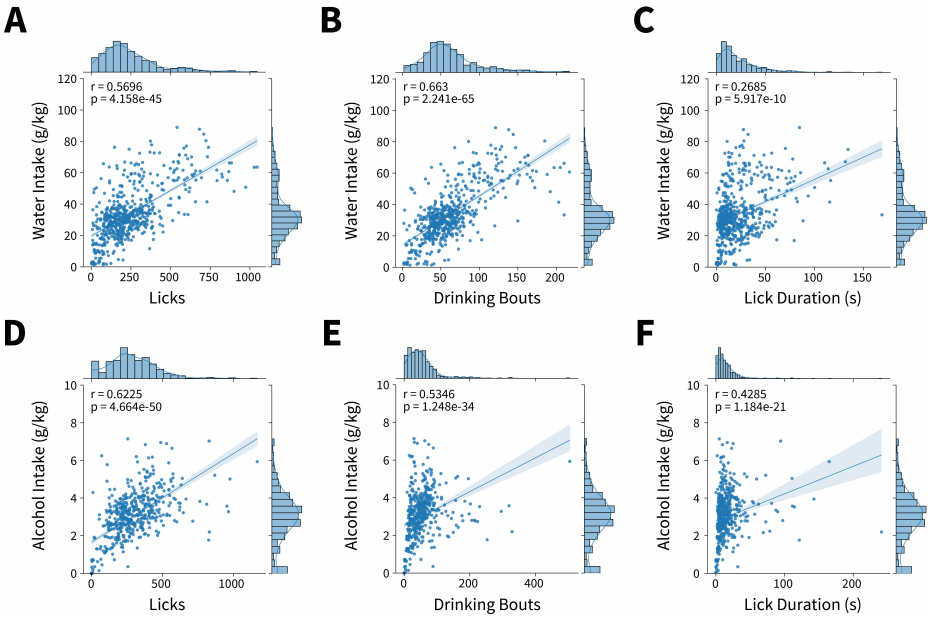

Supplemental Figure 5. Microstructure features measured from lickometers correlate with alcohol and water intakes.
(A) Water licks (Shepherd's pi correlation, r = 0.5696, p = 4.1581e-45), **(B)** bouts (Shepherd's pi correlation, r = 0.6679, p = 1.5517e-66), and **(C)** drinking duration (Shepherd's pi correlation, r = 0.2685, p = 5.9165e-10) per DID session correlate with water intakes. **(D)** Alcohol licks (Shepherd's pi correlation, r = 0.6225, p = 4.6644e-50), **(E)** bouts (Shepherd's pi correlation, r = 0.5343, p = 1.2482e-34), and **(F)** drinking duration (Shepherd's pi correlation, r = 0.4285, p = 1.1841e-21) per DID session correlate with alcohol intakes. Individual datapoints represent a microstructure feature and intake from single Drinking in the Dark session. Data were fit to a linear model represented by a line of best fit with shading indicating ± SEM. Axes histograms display distribution of microstructure features and intakes across all Drinking in the Dark sessions.

Following binge acquisition, animals underwent another three weeks of water or alcohol DID, but the detection of an alcohol or water lick triggered the activation of

the optogenetic probe in a closed-loop manner, delivering blue light (470 nm) to both ChR2 and eGFP controls for the duration of their licking behavior to evoke glutamate release from AIC inputs to the DLS or as a blue light control, respectively (**Figure 2F**). A subset of animals received blue light stimulation stochastically throughout each DID session (see materials and methods), but there were no differences in water or alcohol intakes between closed-loop and open-loop light delivery, so we collapsed on these groupings (**Supplemental figure 6A and B**).

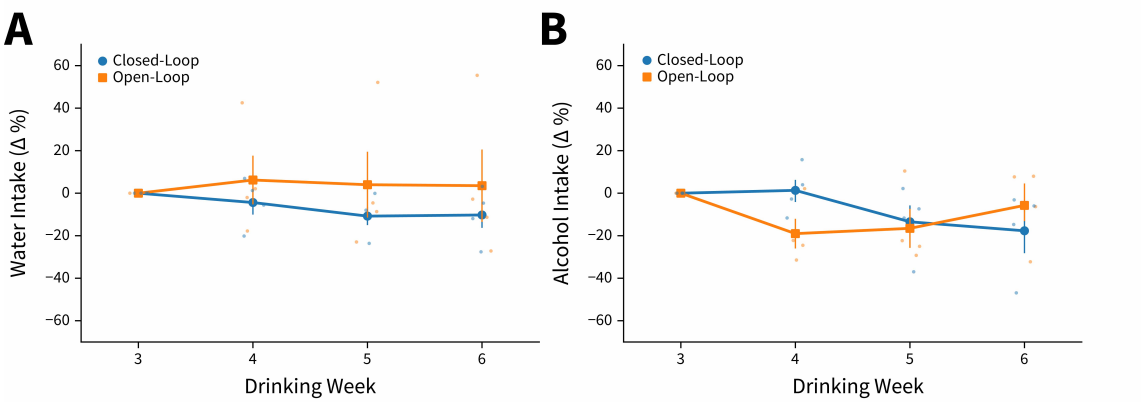

Supplemental Figure 6. ChR2 expressing yoked animals do not differ from closed-loop stimulated animals in alcohol and water intakes.
Intakes during photoexcitation in ChR2 expressing animals do not differ by stimulation delivery paradigm for **(A)** water (two-way mixed ANOVA, Stimulation Paradigm $F_{(1,6)} = 0.6079$, $p = 0.4652$; closed-loop: n = 4 animals, open-loop: n = 4 animals) or **(B)** alcohol (two-way mixed ANOVA, Stimulation Paradigm $F_{(1,6)} = 0.7340$, $p = 0.1268$; closed-loop: n = 4 animals, open-loop: n = 4 animals).

To account for baseline differences between viral expression within fluid type, we summed intakes and microstructure features by week within each animal and displayed these intakes and microstructure features as a percent change from week 3 to determine how photoexciting AIC inputs within the DLS altered intakes and microstructure features. For alcohol and water intake measures for all individual sessions see **supplemental figure 7A and B**.

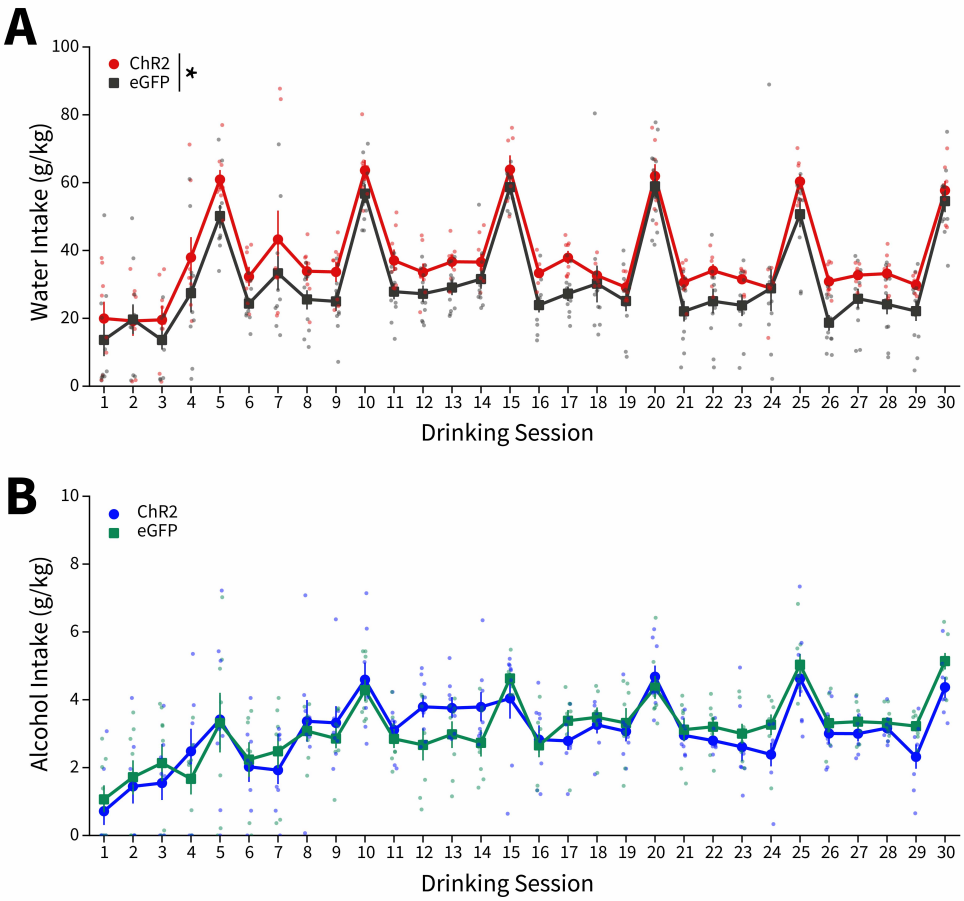

Supplemental Figure 7. Water and Alcohol Intakes for all DID sessions
(A) Water intakes for all sessions (two-way mixed ANOVA, Virus $F_{(1,16)} = 7.2567$, $p = 0.0160$; ChR2: n = 8 animals, eGFP: n = 11 animals). **(B)** Alcohol intakes for all sessions (ChR2: n = 8 animals, eGFP: n = 8 animals).

For binge evaluation (weeks 4 – 6), there was no change in water intake between ChR2 and eGFP controls (**Figure 2G**). Yet, contrary to our initial hypothesis, ChR2-expressing animals drank significantly less alcohol than eGFP controls. Thus, driving glutamate release from AIC inputs within the DLS selectively decreased binge drinking in animals that consumed alcohol, but not water (**Figure 2H**). This was not a product of the in vivo optical stimulation inducing differential plasticity in water and alcohol drinkers. Testing the same stimulation pattern used *in vivo* in brain slices did not produce different effects in slices from water and alcohol drinkers or induce long-lasting glutamatergic plasticity on its own (**Supplemental figure 8**).

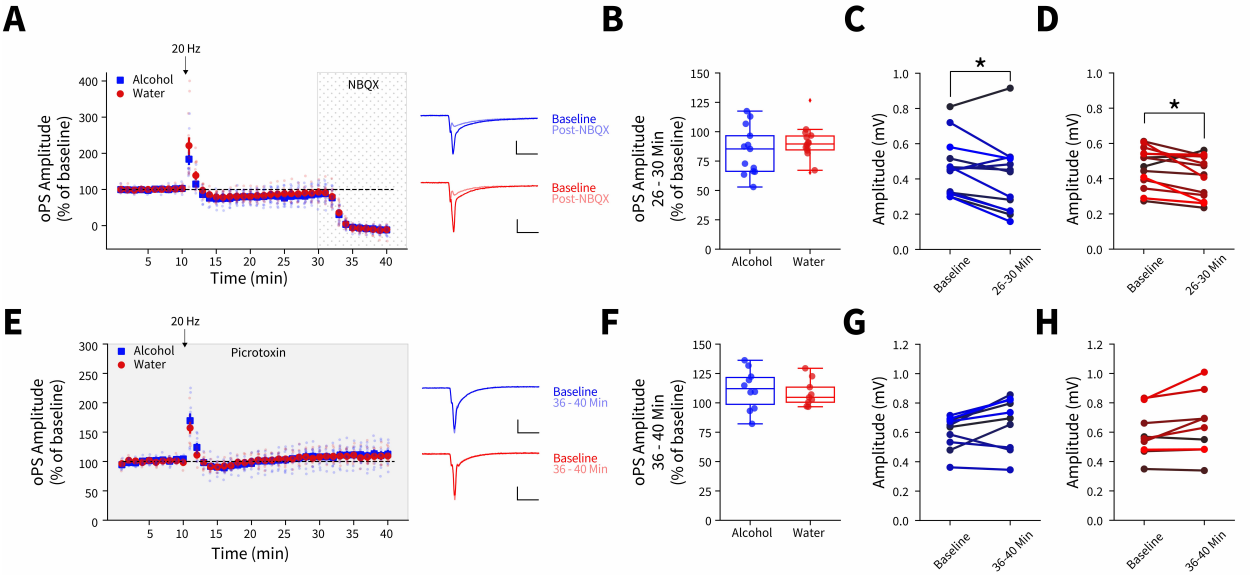

Supplemental Figure 8. Effect of using *in vivo* optogenetic stimulation parameters in brain slices.
(A) The 20 Hz stimulation used for in vivo stimulation does not produce differential responses in AMPA glutamate receptor antagonist (NBQX)-sensitive oPS amplitudes between water- and alcohol-exposed animals (alcohol: 13 recordings, n = 4 animals, water: 14 recordings, n = 5 animals). **(B)** Summary of average 26-30 min oPS amplitudes following 20 Hz stimulation show no group differences between alcohol- and water-exposed animals. 20 Hz stimulation decreased both **(C)** alcohol (paired *t* test, $t_{(12)} = 2.4345$, $p = 0.0315$) and **(D)** water (paired *t* test, $t_{(13)} = 2.6115$, $p = 0.0215$) oPS amplitudes at 26-30 min compared to baseline (0-10 min). **(E)** 20 Hz stimulation does not produce differential responses in oPS amplitudes between water and alcohol exposed animals in the presence of picrotoxin (alcohol: 10 recordings, n = 3 animals, water: 9 recordings, n = 3 animals). **(F)** Summary of average 36-40 min oPS amplitudes following 20 Hz stimulation in the presence of the $GABA_A$ receptor antagonist, picrotoxin, show no group differences between alcohol- and water-exposed animals. In the presence of picrotoxin, there are no differences in baseline (0-10 min) and oPS amplitudes at 36-40 min for **(G)** alcohol- or **(H)** water-exposed animals. These data indicate that 20 Hz stimulation does not induce long-lasting glutamate receptor-mediated synaptic plasticity in either water or alcohol drinking animals.

We reasoned that since driving glutamate release during water DID sessions did not alter intakes, that alcohol-induced plasticity changes at AIC inputs to DLS were a prerequisite for decreasing alcohol intake. To confirm, we photoexcited AIC inputs to the DLS in a separate cohort of animals during binge acquisition (sessions 1-15) to see if animals would decrease their intakes or not acquire stable alcohol intakes. These animals did not show any differences between non-photoexcited alcohol drinkers suggesting alcohol-induced AIC→DLS plasticity changes are necessary to alter binge alcohol intakes (**Supplemental figure 9**).

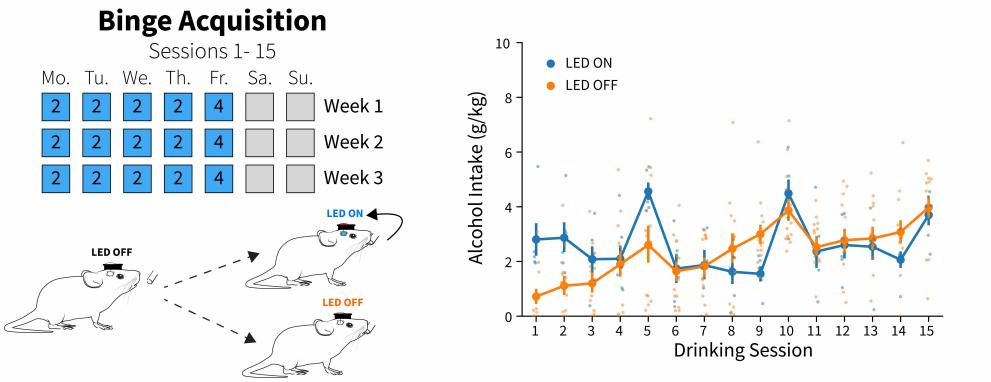

Supplemental Figure 9. Photoexciting AIC inputs to the DLS did not alter alcohol intakes during binge acquisition.
Photoexciting AIC inputs in the DLS did not alter alcohol intakes compared to non-stimulated alcohol drinkers during binge acquisition (two-way mixed ANOVA, LED state $F_{(1,18)} = 0.2484$, $p = 0.6243$; LED ON: n = 6 animals, LED OFF: n = 14 animals).

To quantify behavioral alterations associated with fluid intakes, we analyzed drinking microstructure features across drinking weeks by fluid. For water drinkers, there were no differences between ChR2 and eGFP controls in licks, lick duration, bouts, latency to drink, mean inter-drink interval, or bouts in the first 30 minutes of each DID session (**Figure 3A-F**). As expected for alcohol drinkers, there were significant decreases in licks, lick duration, and bouts in ChR2 compared to eGFP controls (**Figure 3G-I**). For alcohol latency to drink and mean inter-drink-interval there were no significant effects between groups (**Figure 3J and K**), but the number of alcohol bouts in the first 30 minutes (a measurement of 'front-loading' behavior) decreased for ChR2 compared to eGFP controls (**Figure 3L**) (Wilcox et al. 2014).

Although we found significant changes in microstructure features between viral groupings for alcohol drinkers, there were group trends, variability between animals, and many more microstructure features that were not captured in our weekly analyses to characterize intake changes. To more robustly model microstructure changes, we constructed a feedforward artificial neural network using all 18 microstructure features (see **Supplemental Table 1**) from each DID session for all animals to predictively classify both fluid (water v. alcohol) and virus (ChR2 v. eGFP) (**Figure 3M**) (Emmert-Streib et al. 2020). After splitting our dataset into training and testing sets, performing 6-fold stratified cross-validation (to ensure each training fold had a representative proportion of fluid type and viral expression samples), and training the network we achieved an average of 66.13% accuracy (2.6 times better than chance accuracy) on data previously unseen by the model to predict fluid type and viral expression from a single DID session solely from microstructure data (**Figure 3N-O**). Thus, AIC inputs within the DLS govern binge alcohol-related behaviors so strongly that we can reliably predict which animals received specific experimental manipulations based on how they consume fluid from a DID session.

Altogether, our drinking data indicate that alcohol-induced neuroplasticity at AIC inputs to DLS may serve as a gain-of-function that allows these synapses to maintain alcohol consumption. In the absence of alcohol, these synapses seem to play no role in modulating intake behaviors, likely due to the absence of a specific

type of plasticity required to engage or bring these synapses “online.” Once alcohol-induced plasticity at these synapses occurs, it likely enables the governance of alcohol drinking behaviors via complex control over the patterns of licking behavior.

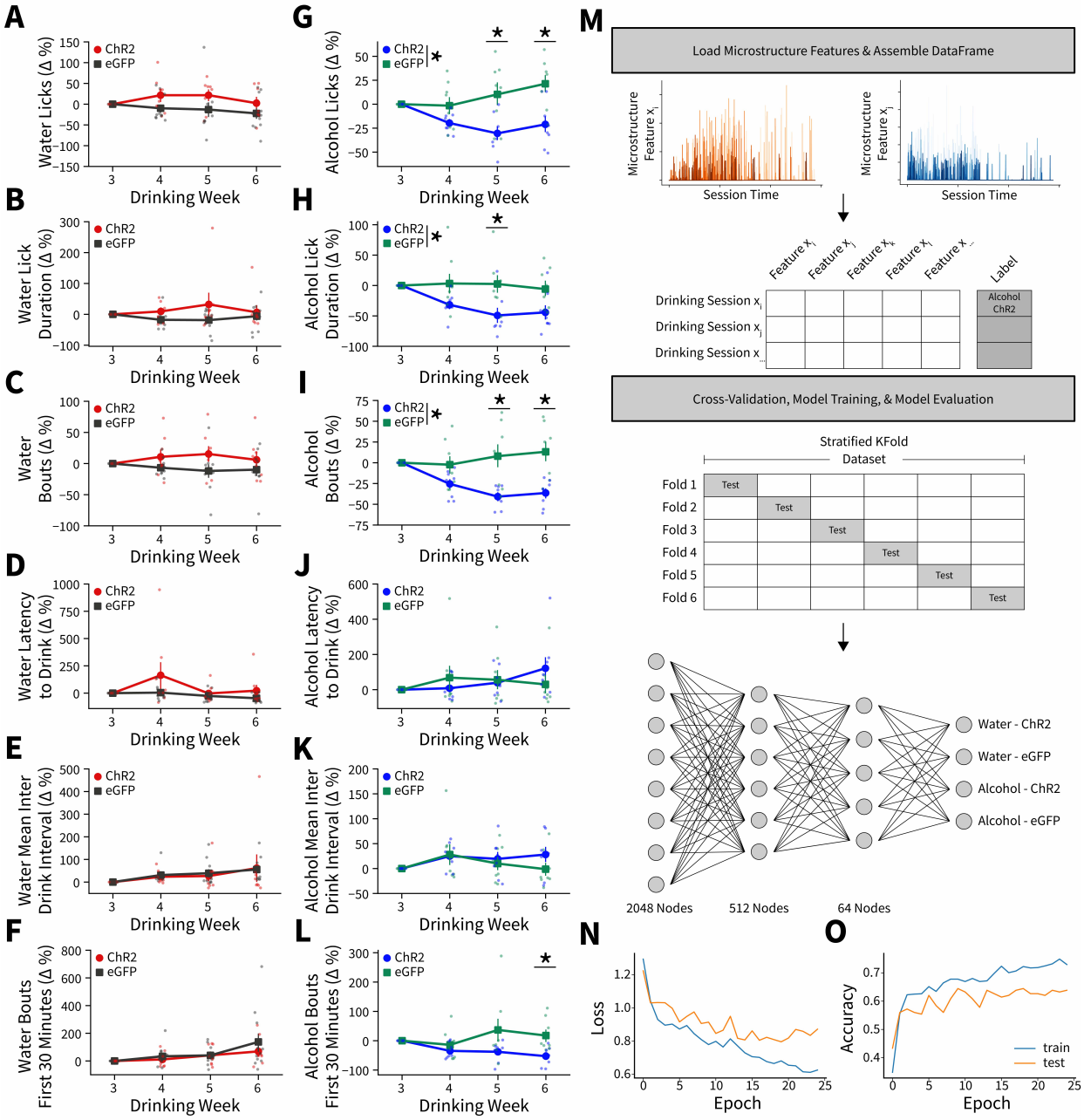

Figure 3 Alterations in drinking microstructure represent significant decreases in alcohol intake and are predictive of AIC→DLS alcohol-induced synaptic plasticity changes. Photoexciting AIC inputs does not alter the (**A**) number of water licks, (**B**) water lick durations, (**C**) water bouts, (**D**) latency to drink water, (**E**) mean inter-drink-interval for water drinking, (**F**) or the number water bouts in the first 30 minutes of the DID session. Photoexciting AIC inputs (**G**) decreases the number of alcohol licks (two-way mixed ANOVA, Virus $F_{(1,14)} = 11.0142$, $p = 0.0051$; Virus x Drinking Week $F_{(3,42)} = 5.8888$, $p = 0.0019$; Week 5 $p = 0.0307$, Week 6 $p = 0.0137$), (**H**) decreases total alcohol lick duration (two-way mixed ANOVA, Virus $F_{(1,14)} = 6.9536$, $p = 0.0195$; Virus x Drinking Week $F_{(3,42)} = 3.8533$, $p = 0.0160$; Week 5 $p = 0.0458$), and (**I**) decreases the number of alcohol bouts (two-way mixed ANOVA, Virus $F_{(1,14)} = 11.2086$, $p = 0.0048$; Virus x Drinking Week

$F_{(3,42)}$ = 9.4893, p = 0.0001; Week 5 p = 0.0135, Week 6 p = 0.0051). (**J**) Modulating AIC inputs does not impact the latency to drink alcohol or (**K**) the mean inter-drink-interval for alcohol drinking, but (**L**) decreases front loading behaviors for alcohol drinking (two-way mixed ANOVA, Virus $F_{(1,14)}$ = 4.2003, p = 0.0596; Virus x Drinking Week $F_{(3,42)}$ = 3.9078, p = 0.0150; Week 6 p = 0.0230). (**M**) Schematic for microstructure feature detection, dataset assembly, cross-validation, and network architecture. (**N**) Loss curve visualization for training and testing data. (**O**) Model accuracy for training and testing data. Error bars indicate ± SEM. All post hoc comparisons are Sidak corrected.

Session	Session Lenght	DIDWeek	Total Licks	Total Lick Duration (s)	Number of Bouts	Mean Licks per Bout	Mean Lick Duration per Bout (s)	Max Lick Duration per Session (s)	Latency to Drink (s)	Mean Inter Drink Interval (s)	Total Licks in First 30 Minutes	Total Lick Duration in First 30 Minutes (s)	Number of Bouts in First 30 Minutes	Mean Licks per Bout in First 30 Minutes	Mean Lick Duration per Bout in First 30 Minutes (s)	Max Lick Duration per Bout in First 30 Minutes (s)	Stimulation State	Fluid x Virus Label
1	2	1	171	26.76	36	4.75	0.73139	3.7	590	187	17	2.36	4	4.25	0.59	1.18	0	1
3	2	1	461	43.83	57	8.0877	0.76123	4.72	980	59	41	6.2	5	8.2	1.24	3.2	0	0
17	2	4	335	48.37	57	5.8772	0.84368	3.47	250	122	92	18.97	19	4.84211	0.99842	3.47	1	2
2	2	1	217	31.94	26	8.3462	1.21423	5.4	170	172	22	3.31	4	5.5	0.8275	2.68	0	1
7	2	1	666	142.86	85	7.8353	1.68071	4.84	240	71	34	5.94	5	6.8	1.188	2.52	0	0
23	2	5	212	22.47	19	11.158	1.18211	3.96	400	282	3	0.38	2	1.5	0.19	0.29	1	1
3	2	1	456	78.58	60	7.6	1.30767	4.21	70	113	111	18.59	21	5.28571	0.88524	2.51	0	0
16	2	4	625	81.08	88	7.1023	0.91977	4.08	40	69	199	23.33	26	7.65385	0.89731	4.08	1	3
14	2	3	372	22.46	46	8.087	0.48804	2.68	580	131	53	2.91	12	4.41667	0.2425	1.22	0	3
28	2	6	209	20.08	18	11.611	1.11444	3.95	340	372	7	2.53	3	2.33333	0.84333	2.49	1	2

Supplemental Table 1. Single DID session microstructure features used for machine learning analysis

An example data frame that contains the 18 microstructure features and label used for machine learning with ten example DID sessions.

We next questioned if the observed decreases in alcohol intake following photoactivation were a product of AIC inputs simply altering behavior in general. In one cohort of animals after the final week of DID, we performed real-time place preference (**Figure 4A**). There were no differences between ChR2 and eGFP controls for time in zone or distance traveled, suggesting photoexciting AIC inputs to the DLS does not alter preference/avoidance behaviors or locomotion (**Figure 4B** and **C**). In a cohort of alcohol-naive animals, we performed a light-dark test (**Figure 4D**). There were no differences between ChR2 and eGFP controls in time spent on the light side of the box across LED epochs, total number of light side entries, or latency to enter the dark side, (**Fig 4. E-G**). Finally, we used optogenetic intercranial self-stimulation to determine if modulating AIC inputs itself was reinforcing (**Figure 4H**). There were no group differences between nosepoking behaviors for photoexcitation (**Figure 4I** and **J**). Altogether, these data indicate that modulating AIC inputs within the DLS does not decrease alcohol intake via changes in reward perception, valence, reinforcement, locomotion, or anxiety-like behavior.

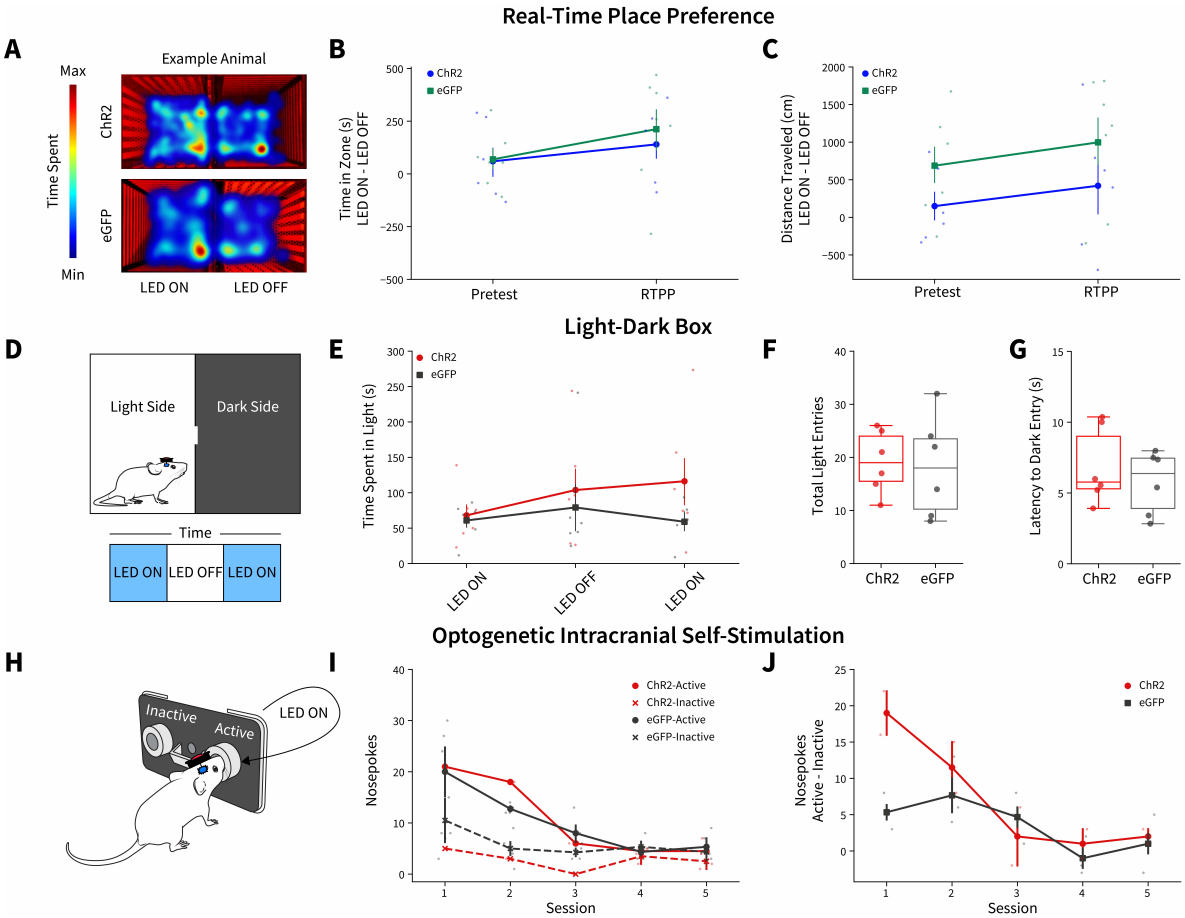

Figure 4 AIC inputs to the DLS do not modulate valence, anxiety-like, or operant responding behaviors

(**A**) Example animal heatmap for real-time place preference assay. Photoexciting AIC inputs within the DLS did not alter (**B**) real-time place preference/avoidance behaviors or (**C**) locomotion during real-time place preference (ChR2: n = 6 animals, eGFP: n = 7 animals). (**D**) Schematic for light-dark box assay. Modulating AIC inputs did not alter (**E**) time spent on light side across LED epochs, (**F**) the number of total light side entries, or (**G**) delays to enter the dark (ChR2: n = 6 animals, eGFP: n = 6 animals). (**H**) Schematic of operant self-stimulation testing. (**I**) Photoexciting AIC inputs did not alter nosepoking behaviors across session. (**J**) Active – Inactive nosepokes do not differ between viral expression when modulating AIC (ChR2: n = 2 animals, eGFP: n = 4 animals). Error bars indicate ± SEM. Box plot whiskers represent inter-quartile range.

In conclusion, we have identified and characterized how binge consumption of alcohol induces changes in synaptic plasticity in a novel corticostriatal circuit that behaviorally governs binge alcohol drinking. Future work is required to determine the mechanisms whereby alcohol-induced neuroplasticity alters circuit function to produce changes in drinking and what specific components of drinking behavior AIC→DLS synapses govern. Nonetheless, the present data suggest that the alcohol-induced synaptic changes described within this circuitry may serve as a critical biomarker for identifying binge alcohol consumption that leads to the future development of AUD, and targeted therapies seeking to modulate this alcohol sensitive circuitry have the potential to immensely impact public health by decreasing binge drinking behaviors.

Materials and Methods:

Animals

Animal care and experimental protocols for this study were approved by the Institutional Animal Care and Use Committee at the Indiana University School of Medicine (IACUC #: 19017) and all guidelines for ethical protocols and care of experimental animals established by the National Institutes of Health (Maryland, USA) were followed. Male C57BL/6J mice were ordered from the Jackson Laboratory (Bar Harbor, Maine, USA). Animals arrived at 6 weeks of age and were allowed to acclimate to the animal facility for at least one week before any surgery was performed. All animals were group-housed (except for mice that underwent Drinking in the Dark experiments as outlined below) in a standard 12-hour light/dark cycle (lights on at 08:00 hours). Humidity in the vivarium was held constant at 50% and food and water were available *ad libitum*.

Stereotaxic Surgeries

All surgeries were conducted under aseptic conditions using an ultra-precise small animal stereotaxic instrument (David Kopf Instruments, USA). Animals were anesthetized using isoflurane (3% for induction, 1.0 – 1.5% for maintenance at a flow rate of 25-35 ml/min of oxygen depending on body weight at the time of surgery). Viral injections were performed using a 33-gauge microinjection needle (Hamilton Company, USA). Animals were treated post operatively for 72 hours with daily injections of carprofen (5 mg/kg) and topical lidocaine on the surgical incision. Animals were allowed to recover for at least one week before behavioral assays began. Animals were assigned to groups randomly and after surgery animal IDs were re-coded to blind experimenters to viral expression status.

<u>For electrophysiology experiments</u>, all mice were injected bilaterally with AAV9-CamKIIa-ChR2(H134R)-EYFP (Addgene, 26969-AAV9) to drive ChR2 expression in the anterior insular cortex (AIC) at coordinates A/P: +2.4, M/L: ±2.30, D/V: −3.00 (50 nl/injection, 25 nl/min infusion rate).

<u>For wireless *in vivo* optogenetic experiments</u>, all mice were injected bilaterally with AAV9-CamKIIa-ChR2(H134R)-EYFP (Addgene, 26969-AAV9) or AAV9-CamKKIIA-eGFP (Addgene, 105541-AAV9) to drive ChR2 expression or eGFP control in AIC at coordinates A/P: +2.4, M/L: ±2.30, D/V: −3.00 (50 nl/injection, 25 nl/min infusion rate). To modulate AIC inputs in the dorsolateral striatum (DLS), mice were unilaterally implanted with a wireless probe (4 mm depth, 470 nm blue light LED - Neurolux, USA) at coordinates A/P: +0.7, M/L: ±1.55, D/V: −2.5. The LED orientation allowed for light to travel from anterior DLS to posterior DLS and ensured minimization of off-target light activation of AIC cell bodies while maximizing light coverage for AIC input innervation in the DLS. Probes were placed in either the right or left DLS, but there was no lateralization effect on alcohol or water intake, thus data are presented collapsed on probe location. Probes were secured to the skull using ethyl cyanoacrylate (LOCTITE® 444, Henkel, USA) and the skin was closed over the top of the probe using Vetbond tissue adhesive (3M, USA).

Drinking in the Dark

The Drinking in the Dark (DID) paradigm was based on the original DID procedure (Thiele and Navarro 2014) with two modifications. First, there were four 2-hour DID sessions (Monday – Thursday) and one 4-hour DID session (Friday) and second, all DID sessions were performed out of a single bottle of water or alcohol (20% v/v in water) via lickometers (described below) inserted into the cage at the beginning of the DID session, which were removed at the end of the DID session. Mice had *ab libitum* access to their standard water bottles at all other times.

To summarize the performed procedures, after animals recovered from surgery, they were singly housed and allowed to acclimate in a reverse 12-hour dark/light cycle (lights off at 06:00 hours) for one week. Three hours into the dark cycle (09:00 hours) the standard water bottle was removed from the cage and the lickometer was inserted into the cage after the fluid bottle was weighed for two or four hours depending on the test day. Following the completion of two- or four-hour access, the lickometers were removed and the fluid bottles were weighed immediately after the session. Grams per kg (g/kg) of water and alcohol were computed from the difference in bottle weight and the density of water or 20% alcohol in water. Mice were weighed post-DID session on Monday, Wednesday, and Friday (Tuesday and Thursday weights were equivalent to Monday and Wednesday, respectively). For Saturday and Sunday, the mice had no access to the lickometers as no procedures were performed. These one-week repeating DID cycles are referred to as “Drinking Weeks.”

Water and alcohol intakes for study inclusion were determined by summing the intake across the first 15 DID sessions. Animals that fell outside of the lower interquartile range for their respective fluid type were excluded from the study for not consuming enough water or alcohol in the binge acquisition period. Only 1 alcohol animal was removed from the study for failure to meet this criterion as it only consumed a total of 1.28 g/kg of alcohol across all 15 DID sessions.

Blood alcohol concentration

In a subset of animals following all DID sessions as to not disturb drinking, retro-orbital blood samples were taken after an additional two-hour DID session. Blood alcohol concentrations were determined via gas chromatography (GC-2010 plus, Shimadzu, Japan) and correlated with respective alcohol intakes from that session.

Electrophysiology

Brain slices were prepared 24 hours after the completion of the mice’s final sessions during week 4 (sessions 16-20) of DID. Mice were anesthetized with isoflurane and then immediately killed via decapitation. The brain was rapidly dissected out and placed in an ice-cold cutting solution containing (in mM): 194 sucrose, 30 NaCl, 26 $NaHCO_3$, 10 Glucose, 4.5 KCl, 1.2 NaH_2PO_4, and1 $MgCl_2$, saturated with a 95/5% O_2/CO_2 mixture. Brain slices containing the DLS were made at a thickness of 280 µm on a VT1200S vibratome (Leica, Germany). Slices were incubated in artificial cerebrospinal fluid (aCSF) containing (in mM): 124 NaCl, 26 $NaHCO_3$, 10 Glucose, 4.5 KCl, 2 $CaCl_2$, 1.2 NaH_2PO_4, 1 $MgCl_2$ (310–320 mOsm) saturated with a 95/5% O_2/CO_2 mixture at 30 °C for 1 h after which they were moved to incubate at room temperature until recording.

DLS brain slices were transferred to a recording chamber continuously perfused with 95/5% O2/CO2-saturated aCSF solution at a rate of 1-2 mL/min at 29–32 C°.

DLS brain slices were visualized on a BX51WI microscope (Olympus Corporation of America, USA). Whole-cell patch clamp electrophysiological recordings were made from medium spiny neurons (MSNs) in the voltage-clamp configuration. Recordings were made using a Multiclamp 700B amplifier and a 1550B Digidata digitizer (Molecular Devices, USA). Glass patch pipettes (borosilicate with filament, 2.0–3.5MΩ resistance, World Precision Instruments, USA) were made using a P-1000 micropipette puller (Sutter Instruments, USA). Pipette internal solution contained (in mM) 120 CsMeSO3, 10 HEPES, 10 TEA-Cl, 5 lidocaine bromide, 5 NaCl, 4 Mg-ATP, 1.1 EGTA, and 0.3 Na-GTP (pH 7.2, 290–310 mOsm). MSN identity was determined visually based on soma size and confirmed via measures of membrane resistance and capacitance. MSNs were constantly voltage clamped at −60 mV, using sampling rate of 10kHz and low-Bessel filter 2kHz. In order to isolate excitatory transmission, picrotoxin (50 μM) was added to the aCSF solution for whole cell recordings and a subset of field recordings. Extracellular field recordings were used to measure network responses using glass micropipettes filled with 1M NaCl. Both whole cell patch pipettes and field recording pipettes were placed in the regions of the DLS where AIC innervation was the most dense (**Supplemental figure 1**) for recordings. Data were acquired using Clampex 10.3 (Molecular Devices,USA). For whole cell recordings, series resistance was monitored throughout the experiment. Cells with series resistances greater than 25MΩ or that changed more than 15% during recording were excluded from data analyses.

Optically-evoked excitatory post synaptic currents (oEPSCs) or optically-evoked population spikes (oPSs) were produced in DLS brain slices using 5 ms 470 nm blue LED light pulses delivered via field illumination through the microscope objective. oEPSCs and oPSs were evoked every 30 s. Stimulus-response measures of oEPSC and oPS amplitudes were performed by increasing the intensity of blue LED light from 0 up to 1.15 mW. For AMPA/NMDA and paired-pulse ratio (PPR) whole cell recording measures, light intensity was initially adjusted to produce stable oEPSCs of 200–600 pA amplitude after which experimental recordings were begun. Optical AMPA/NMDA (oAMPA/oNMDA) current ratio recordings were measured by first holding the cell at −80 mV and optically evoking an AMPAR-mediated EPSC. The NMDAR current was then determined by shifting the membrane potential to +40 mV and optically evoking an EPSC. Since the AMPAR component of oEPSCs at −80 mV was not apparent at 100 ms following the optical stimulus (the measured current rapidly returned to baseline), we calculated the NMDAR-mediated portion of the oEPSC at +40 mV as the average of the measured current over the following 25 ms (100–125 ms post-stimulus), similar to our previously published protocol (Fritz et al. 2018). oPPRs were measured by performing two optical stimulations separated by 50-200 ms averaging three technical replicates. oPPR was calculated by taking the average amplitude of the second pulses (using tail current as baseline) and dividing it by the average amplitude of the first pulses (using pre-stimulation current as baseline). Non-optically evoked spontaneous EPSCs (sEPSCs) were also measured using whole cell voltage clamp recordings, with MSNs held at -60 mV using sampling rate of 50 kHz . sEPSCs were measured over the course of a 2 min gap-free recording. sEPSC amplitude, frequency, and decay and rise times were computed using Minianalysis (Synaptosoft, USA).

Histology

Animals were anaesthetized with isoflurane and trans-cardially perfused with 15 ml of ice-cold phosphate buffered saline (PBS) followed by 25 ml of ice-cold 4% paraformaldehyde in PBS (PFA). Animals were decapitated and the brain was extracted and placed in 4% PFA for 24 hours. Brains were then transferred to 30% sucrose solution until they sank after which they were sectioned on a vibratome at a section thickness of 50 µm. Brain sections were mounted in serial order on glass microscope slides and stained with 4′,6-diamidino-2-phenylindole (DAPI) to visualize nuclei. Fluorescent images were captured on a BZ-X810 fluorescent microscope (Keyence, USA) using 4X and 20X air objectives. Injection site, viral expression, and the location of optogenetic probe implantations were determined from matching images to the Reference Allen Mouse Brain Atlas. Animals that did not have viral expression in the brain regions of interest and/or did not have optogenetic probe placements within the brain region of interest as confirmed by histology were excluded from the study.

Lickometers

All alcohol and water drinking experiments were performed out of custom-built home cage fluid monitors (i.e “lickometers”) that were constructed as described (Godynyuk et al. 2019) with the following modifications. Liquid monitoring was constantly sampled as a function of the state (open v closed) of an infrared beam directly in front of the fluid bottle valve, but data was only written to device memory at minimum every two seconds. Therefore, any tube interaction within a two second window (defined as a drinking bout) was recorded as the total number of beam breaks (defined as licks) for the total duration that the beam was broken (defined as lick duration) within that bout. Drinking bouts could be longer than two seconds, but never shorter.

The lickometers can hold two bottles, although we only used one for each device during these experiments. We randomized the bottle side location across animals and found no effect on drinking, thus data are presented collapsed on bottle side.

Lickometer data was cleaned by fitting a linear model comparing the number of licks by the lick duration within each bout for every DID session performed by each animal. Bouts that had a residual value of greater than or less than 3 from model fit were removed. This cleaning procedure removed bouts that were due to slow leaks (a new tube was used if a leak was detected for the next DID session) or chews on the bottles. A total of 3,928,956 bouts were recorded across all experiments, and after cleaning 3,927,570 remained (99.9647% of bouts remained) showing that almost all bottle contacts were directed drinking behaviors, and that chews and leaks were rare.

For wireless *in vivo* optogenetic experiments that utilized lickometers for closed-loop control during DID sessions, the lickometer’s BNC out was connected to a TTL port on the Neurolux optogenetics system such that when a lick occurred, for the entire duration of the lick, a voltage change was sent from the lickometer to turn on the optogenetics probe. Optogenetic stimulation was delivered at 20 Hz with 5 mW of light power at 470 nm for the entire duration of the beam break.

In a subset of animals, we also performed yoked controls such that yoked animals received optogenetic stimulation at stochastic time points during DID sessions. The yoked controls' stimulations were dependent on the drinking activity of some other animal in the room during the DID session to ensure the amount of stimulation and type (length, interval, etc.) was similar across groupings. There were no differences in intake by yoked status for water or alcohol, thus the data are presented collapsed on yoked and closed-loop stimulation. This finding suggests that changes in alcohol intake driven by optogenetic manipulations may be generalizable to when alcohol is accessible or at timepoints near alcohol consumption behaviors, and not necessarily linked to closed-looped stimulation during licking activity.

Microstructure feature analyses

Using licks, lick duration, bouts, and the timestamps when these events occurred during the DID session, we calculated other drinking features such as latency to drink (time to first bream break after session initiation) and mean inter-drink interval time per session (the mean time between bouts within each DID session). We also calculated features for events in the first 30 minutes of each DID session as a measure of front-loading behavior. Finally, we used maximum values (max bout length, max licks per bout, etc.) to characterize microstructure features within DID sessions.

Machine Learning

A feedforward artificial neural network was used to determine if microstructure features from a single DID session could predict the experimental manipulations across fluid type (alcohol v water) and viral expression (ChR2 v eGFP). To bolster our predictive capabilities, we used all 18 microstructure features we computed per DID session.

Features were concatenated across all animals and DID sessions into a single data frame and categorical labels were one-hot encoded (see **Table S1** for examples). Data were normalized to a range of 0 – 1 before cross-validation using stratified k-fold (k =6) to ensure the unequal proportion of fluid x virus labels in the dataset did not influence model training predictions. Each shuffled fold contained 832 training examples and 166 testing samples. The sequential network architecture contained 2048 nodes in the first layer, 512 nodes in the second layer, 64 nodes in third layer, and an output layer of 4 nodes. We used a rectified linear unit (ReLU) activation function for the first three layers and a softmax activation function for the final output layer. The model was compiled using an Adam optimizer and loss was scored using categorical cross entropy. After training all 6 folds, the average testing accuracy on data previously unseen by the model was 66.13% with a maximum of 70.48% accuracy for one of the training folds.

Real-time place preference

One week after the final DID session (session 30), animals were subjected to a real-time place preference (RTPP) assay to determine if photoexciting AIC inputs altered valence states that could explain differences in alcohol behaviors. Animals were placed in an arena (40 cm x 20 cm x 30 cm) with a divider down the middle that contained a cutout so mice could freely passthrough from one side to the other. One side of the arena contained a mesh floor with vertical stripped walls and the other with wire floor and horizontal stripped walls. All testing was performed in the dark using red light and infrared cameras to capture behavioral videos. Two boxes were used, each with

counterbalanced LED ON sides that triggered the activation of the optogenetic probe to deliver 20 Hz 470 nm light pulses at 5 mW when entry into that side of the arena occurred for the entire duration the animal was in that side of the arena. For the pretest day, animals were placed in the arena for 20 minutes with no optogenetic activation regardless of their location in the arena. On the RTPP testing day the same procedure was repeated except the LED ON side of the box triggered optogenetic stimulation. All location and locomotion data were computed using EthoVision XT (V15 – Noldus, USA) from a camera placed directly above the arena which measured the center of the animal as it freely behaved across testing.

Light dark box

A light dark box assay was used in a separate cohort of alcohol-naïve mice to determine if photoexciting AIC inputs could alter anxiety-related behaviors. Mice were placed into an arena (40 cm x 40 cm x 30 cm) that was split in half with a covered divider that contained a cutout so mice could freely pass through from one side to the other. The open side of the box was brightly lit (300-500 lumens) with overhead light and the other covered side registered dimly lit (0-10 lumens). The 15-minute session consisted of 3 epochs (LED ON, LED OFF, LED ON) for 5 minutes each. During the LED ON epochs, optogenetic stimulation was delivered at 20 Hz with 470 nm light pulses at 5 mW for the duration of the epoch. Animals were placed in the corner furthest from the dark entry to begin the assay. All animal tracking data was computed using EthoVision XT (V15 – Noldus, USA) from a camera placed directly above the arena which measured the center of the animal as it freely behaved across testing.

Intracranial self-stimulation

Intracranial self-stimulation was used to determine if photoactivation of AIC inputs could maintain an operant response. Intracranial self-stimulation was performed in a homecage (30 cm x 15 cm x 15 cm) with a FED3 device (Matikainen-Ankney et al. 2021). Each FED3 device has two nose poke ports (“active” and “inactive”). Animals were pretrained for one week with FED3 devices on a fixed-ratio 5 (FR5) schedule to deliver a chocolate pellet. This allowed for animals to nose poke without bait in the active port for self-stimulation testing. Following the week of pretraining, responding in the active port was reinforced with photoactivation on a fixed-ratio 1 schedule and resulted in light delivery (5 mW of 470 nm light in 25 ms pulses for a total of 20 pulses) as well as presentation of a tone (4 kHz for 300 ms) and illumination of a cue light bar located below the active nose port. The inactive port resulted in no photoactivation, tone, or light cue. Animals were run for 5 sessions, each one hour long. No pellets were delivered during self-stimulation testing.

Modeling and Statistics

Sample sizes for all experiments were determined based on previously published experimental findings for electrophysiology and in vivo behavioral, assays such as Drinking in the Dark (Munoz et al. 2018).

Data preprocessing and machine learning modeling utilized SciPy (Virtanen et al. 2020), Statsmodels (Seabold and Perktold 2010), Scikit-learn (Pedregosa et al. 2011), and TensorFlow (Abadi et al. 2016). Statistical analyses were performed using GraphPad Prism (GraphPad Software - V9.2, USA) and pingouin (V0.5.0, (Vallat 2018)). Data

visualization used matplotlib (Hunter 2007) and seaborn (Waskom 2021) libraries. For time series or repeated measures, we used two-way mixed ANOVAs, which represented time (session or week) or the repeated factor (light power, etc.) as the repeated, within-subject variable, and the factor (fluid type, viral expression, bottle side, etc.) as the between-subjects factor. All two-way mixed ANOVA data were tested to see if variances between factors were equal and normal using the Levene test. If there was a main effect for factor, we used pairwise t-tests to determine post-hoc significance and p-values were Sidak corrected. For correlations between two variables, we tested multivariate normality using the Henze-Zirkler test. If samples were normal, we used a Pearson correlation to report r and p-values. If samples failed normality testing, we used a Shepherd pi correlation that returned the Spearman correlation after removing bi-variate outliers. For tests of two factors, we used unpaired Welch two-tailed t-tests to correct for unequal sample sizes or paired t-tests. All significance thresholds were placed at $p < 0.05$ and all data and model fits are shown as mean ± standard error (68% confidence interval) of the mean (SEM) or by box plot with error bars indicating the interquartile range (IQR). Data points beyond IQRs are represented as diamonds.

Acknowledgments:

We thank Kaitlin C. Reeves, Gonzalo Viana Di Prisco, Brandon M. Fritz, and Fuqin Yin for experimental assistance and Erin A. Newell for technical assistance. We also thank Lex Kravitz and Ethan Tyler for modified drawings that were accessed via scidraw.io.

Funding:

National Institutes of Health grant R01AA027214 (BKA)

National Institutes of Health grant F31AA029297 (DLH)

National Institutes of Health grant F30AA028687 (GGG)

National Institutes of Health grant T32AA07462 (DLH)

Stark Neurosciences Research Institute (BKA, DLH, GGG)

Indiana University Health (BKA)

Author contributions:

Conceptualization: DLH, BKA

Methodology: DLH, BM, BKA

Investigation: DLH, BM, TP

Visualization: DLH, BM, TP

Software: DLH

Funding acquisition: DLH, GGG, BKA

Project administration: DLH, BKA

Supervision: DLH, BM, GGG, BKA

Writing – original draft: DLH

Writing – review & editing: DLH, BM, GGG, BKA

Competing interests:

Authors declare that they have no competing interests.

Data and materials availability:

All experimental data are available in the main text or the supplementary materials. Microstructure analysis and machine learning code is available at github.com/dlhagger

References:

Abadi, Martín, Paul Barham, Jianmin Chen, Zhifeng Chen, Andy Davis, Jeffrey Dean, Matthieu Devin, Sanjay Ghemawat, Geoffrey Irving, Michael Isard, Manjunath Kudlur, Josh Levenberg, Rajat Monga, Sherry Moore, Derek G. Murray, Benoit Steiner, Paul Tucker, Vijay Vasudevan, Pete Warden, Martin Wicke, Yuan Yu, and Xiaoqiang Zheng. 2016. "TensorFlow: a system for large-scale machine learning." In *Proceedings of the 12th USENIX conference on Operating Systems Design and Implementation*, 265–83. Savannah, GA, USA: USENIX Association.

Addolorato, G., G. A. Vassallo, G. Antonelli, M. Antonelli, C. Tarli, A. Mirijello, A. Agyei-Nkansah, M. C. Mentella, D. Ferrarese, V. Mora, M. Barbara, M. Maida, C. Camma, A. Gasbarrini, and Consortium Alcohol Related Disease. 2018. 'Binge Drinking among adolescents is related to the development of Alcohol Use Disorders: results from a Cross-Sectional Study', *Sci Rep*, 8: 12624.

Barker, J. M., L. H. Corbit, D. L. Robinson, C. M. Gremel, R. A. Gonzales, and L. J. Chandler. 2015. 'Corticostriatal circuitry and habitual ethanol seeking', *Alcohol*, 49: 817-24.

Burnham, N. W., C. N. Chaimowitz, C. C. Vis, A. P. Segantine Dornellas, M. Navarro, and T. E. Thiele. 2021. 'Lateral hypothalamus-projecting noradrenergic locus coeruleus pathway modulates binge-like ethanol drinking in male and female TH-ires-cre mice', *Neuropharmacology*, 196: 108702.

Centanni, S. W., A. C. Janes, D. L. Haggerty, B. Atwood, and F. W. Hopf. 2021. 'Better living through understanding the insula: Why subregions can make all the difference', *Neuropharmacology*, 198: 108765.

Chung, T., K. G. Creswell, R. Bachrach, D. B. Clark, and C. S. Martin. 2018. 'Adolescent Binge Drinking Developmental Context and Opportunities for Prevention', *Alcohol Research-Current Reviews*, 39: 5-15.

Corbit, L. H., H. Nie, and P. H. Janak. 2012. 'Habitual alcohol seeking: time course and the contribution of subregions of the dorsal striatum', *Biol Psychiatry*, 72: 389-95. 2014. 'Habitual responding for alcohol depends upon both AMPA and D2 receptor signaling in the dorsolateral striatum', *Front Behav Neurosci*, 8: 301.

Dornellas, A. P. S., N. W. Burnham, K. L. Luhn, M. V. Petruzzi, T. E. Thiele, and M. Navarro. 2021. 'Activation of locus coeruleus to rostromedial tegmental nucleus (RMTg) noradrenergic pathway blunts binge-like ethanol drinking and induces aversive responses in mice', *Neuropharmacology*, 199: 108797.

Emmert-Streib, Frank, Zhen Yang, Han Feng, Shailesh Tripathi, and Matthias Dehmer. 2020. 'An Introductory Review of Deep Learning for Prediction Models With Big Data', *Frontiers in Artificial Intelligence*, 3.

Ferguson, L. B., L. Zhang, D. Kircher, S. Wang, R. D. Mayfield, J. C. Crabbe, R. A. Morrisett, R. A. Harris, and I. Ponomarev. 2019. 'Dissecting Brain Networks Underlying Alcohol Binge Drinking Using a Systems Genomics Approach', *Mol Neurobiol*, 56: 2791-810.

Fritz, B. M., B. Muñoz, F. Yin, C. Bauchle, and B. K. Atwood. 2018. 'A High-fat, High-sugar 'Western' Diet Alters Dorsal Striatal Glutamate, Opioid, and Dopamine Transmission in Mice', *Neuroscience*, 372: 1-15.

Godynyuk, E., M. N. Bluitt, J. R. Tooley, A. V. Kravitz, and M. C. Creed. 2019. 'An Open-Source, Automated Home-Cage Sipper Device for Monitoring Liquid Ingestive Behavior in Rodents', *eNeuro*, 6: ENEURO.0292-19.2019.

Gogolla, Nadine. 2017. 'The insular cortex', *Current Biology*, 27: R580-R86.

Hunnicutt, B. J., B. C. Jongbloets, W. T. Birdsong, K. J. Gertz, H. Zhong, and T. Mao. 2016. 'A comprehensive excitatory input map of the striatum reveals novel functional organization', *Elife*, 5.

Hunter, John D. 2007. 'Matplotlib: A 2D Graphics Environment', *Computing in Science & Engineering*, 9: 90-95.

Hwa, L., J. Besheer, and T. Kash. 2017. 'Glutamate plasticity woven through the progression to alcohol use disorder: a multi-circuit perspective', *F1000Res*, 6: 298.

Jackman, S. L., and W. G. Regehr. 2017. 'The Mechanisms and Functions of Synaptic Facilitation', *Neuron*, 94: 447-64.

Kanny, D., T. S. Naimi, Y. Liu, H. Lu, and R. D. Brewer. 2018. 'Annual Total Binge Drinks Consumed by U.S. Adults, 2015', *Am J Prev Med*, 54: 486-96.

Koob, G. F., and N. D. Volkow. 2010. 'Neurocircuitry of addiction', *Neuropsychopharmacology*, 35: 217-38.

Levine, O. B., M. J. Skelly, J. D. Miller, J. K. Rivera-Irizarry, S. A. Rowson, J. F. DiBerto, J. A. Rinker, T. E. Thiele, T. L. Kash, and K. E. Pleil. 2021. 'The paraventricular thalamus provides a polysynaptic brake on limbic CRF neurons to sex-dependently blunt binge alcohol drinking and avoidance behavior in mice', *Nat Commun*, 12: 5080.

Lovinger, D. M., and V. A. Alvarez. 2017. 'Alcohol and basal ganglia circuitry: Animal models', *Neuropharmacology*, 122: 46-55.

Manz, K. M., D. Ghose, B. D. Turner, A. Taylor, J. Becker, C. A. Grueter, and B. A. Grueter. 2020. 'Calcium-Permeable AMPA Receptors Promote Endocannabinoid Signaling at Parvalbumin Interneuron Synapses in the Nucleus Accumbens Core', *Cell Rep*, 32: 107971.

Matikainen-Ankney, B. A., T. Earnest, M. Ali, E. Casey, J. G. Wang, A. K. Sutton, A. A. Legaria, K. M. Barclay, L. B. Murdaugh, M. R. Norris, Y. H. Chang, K. P. Nguyen, E. Lin, A. Reichenbach, R. E. Clarke, R. Stark, S. M. Conway, F. Carvalho, R. Al-Hasani, J. G. McCall, M. C. Creed, V. Cazares, M. W. Buczynski, M. J. Krashes, Z. B. Andrews, and A. V. Kravitz. 2021. 'An open-source device for measuring food intake and operant behavior in rodent home-cages', *Elife*, 10: e66173.

Mokdad, A. H., J. S. Marks, D. F. Stroup, and J. L. Gerberding. 2004. 'Actual causes of death in the United States, 2000', *JAMA*, 291: 1238-45.

Munoz, B., B. M. Fritz, F. Yin, and B. K. Atwood. 2018. 'Alcohol exposure disrupts mu opioid receptor-mediated long-term depression at insular cortex inputs to dorsolateral striatum', *Nat Commun*, 9: 1318.

Munoz, B., D. L. Haggerty, and B. K. Atwood. 2020. 'Synapse-specific expression of mu opioid receptor long-term depression in the dorsomedial striatum', *Sci Rep*, 10: 7234.

Patrick, M. E., J. E. Schulenberg, M. E. Martz, J. L. Maggs, P. M. O'Malley, and L. D. Johnston. 2013. 'Extreme binge drinking among 12th-grade students in the United States: prevalence and predictors', *JAMA Pediatr*, 167: 1019-25.

Patton, M. S., M. Heckman, C. Kim, C. Mu, and B. N. Mathur. 2021. 'Compulsive alcohol consumption is regulated by dorsal striatum fast-spiking interneurons', *Neuropsychopharmacology*, 46: 351-59.

Patton, Mary H., Aparna P. Shah, and Brian N. Mathur. 2016. 'Alcohol Effects on the Dorsal Striatum.' in Jean-Jacques Soghomonian (ed.), *The Basal Ganglia: Novel Perspectives on Motor and Cognitive Functions* (Springer International Publishing: Cham).

Pedregosa, Fabian, Gaël Varoquaux, Alexandre Gramfort, Vincent Michel, Bertrand Thirion, Olivier Grisel, Mathieu Blondel, Peter Prettenhofer, Ron Weiss, and Vincent Dubourg. 2011. 'Scikit-learn: Machine learning in Python', *the Journal of machine Learning research*, 12: 2825-30.

Rinker, J. A., S. A. Marshall, C. M. Mazzone, E. G. Lowery-Gionta, V. Gulati, K. E. Pleil, T. L. Kash, M. Navarro, and T. E. Thiele. 2017. 'Extended Amygdala to Ventral Tegmental Area Corticotropin-Releasing Factor Circuit Controls Binge Ethanol Intake', *Biol Psychiatry*, 81: 930-40.

Seabold, Skipper, and Josef Perktold. 2010. "Statsmodels: Econometric and statistical modeling with python." In *Proceedings of the 9th Python in Science Conference*, 61. Austin, TX.

Shin, G., A. M. Gomez, R. Al-Hasani, Y. R. Jeong, J. Kim, Z. Xie, A. Banks, S. M. Lee, S. Y. Han, C. J. Yoo, J. L. Lee, S. H. Lee, J. Kurniawan, J. Tureb, Z. Guo, J. Yoon, S. I. Park, S. Y. Bang, Y. Nam, M. C. Walicki, V. K. Samineni, A. D. Mickle, K. Lee, S. Y. Heo, J. G. McCall, T. Pan, L. Wang, X. Feng, T. I. Kim, J. K. Kim, Y. Li, Y. Huang, R. W. th Gereau, J. S. Ha, M. R. Bruchas, and J. A. Rogers. 2017. 'Flexible Near-Field Wireless Optoelectronics as Subdermal Implants for Broad Applications in Optogenetics', *Neuron*, 93: 509-21 e3.

Siciliano, C. A., H. Noamany, C. J. Chang, A. R. Brown, X. Chen, D. Leible, J. J. Lee, J. Wang, A. N. Vernon, C. M. Vander Weele, E. Y. Kimchi, M. Heiman, and K. M. Tye. 2019. 'A cortical-brainstem circuit predicts and governs compulsive alcohol drinking', *Science*, 366: 1008-12.

Thiele, T. E., and M. Navarro. 2014. '"Drinking in the dark" (DID) procedures: a model of binge-like ethanol drinking in non-dependent mice', *Alcohol*, 48: 235-41.

Vallat, Raphael. 2018. 'Pingouin: statistics in Python', *Journal of Open Source Software*, 3: 1026.

Virtanen, P., R. Gommers, T. E. Oliphant, M. Haberland, T. Reddy, D. Cournapeau, E. Burovski, P. Peterson, W. Weckesser, J. Bright, S. J. van der Walt, M. Brett, J. Wilson, K. J. Millman, N. Mayorov, A. R. J. Nelson, E. Jones, R. Kern, E. Larson, C. J. Carey, I. Polat, Y. Feng, E. W. Moore, J. VanderPlas, D. Laxalde, J. Perktold, R. Cimrman, I. Henriksen, E. A. Quintero, C. R. Harris, A. M. Archibald, A. H. Ribeiro, F. Pedregosa, P. van Mulbregt, and Contributors SciPy. 2020. 'SciPy 1.0: fundamental algorithms for scientific computing in Python', *Nat Methods*, 17: 261-72.

Wall, N. R., M. De La Parra, E. M. Callaway, and A. C. Kreitzer. 2013. 'Differential innervation of direct- and indirect-pathway striatal projection neurons', *Neuron*, 79: 347-60.

Waskom, Michael L. 2021. 'Seaborn: statistical data visualization', *Journal of Open Source Software*, 6: 3021.

Wilcox, M. V., V. C. Cuzon Carlson, N. Sherazee, G. M. Sprow, R. Bock, T. E. Thiele, D. M. Lovinger, and V. A. Alvarez. 2014. 'Repeated binge-like ethanol drinking alters ethanol drinking patterns and depresses striatal GABAergic transmission', *Neuropsychopharmacology*, 39: 579-94.